

# Formation of very hard electron and gamma-ray spectra of flat spectrum radio quasar in fast-cooling regime

Dahai Yan<sup>1\*</sup>, Li Zhang<sup>2†</sup>, Shuang-Nan Zhang<sup>1‡</sup>

<sup>1</sup>Key Laboratory of Particle Astrophysics, Institute of High Energy Physics, Chinese Academy of Sciences, Beijing 100049, China

<sup>2</sup>Department of Astronomy, Key Laboratory of Astroparticle Physics of Yunnan Province, Yunnan University, Kunming, 650091, China

Accepted XXX. Received YYY; in original form ZZZ

## ABSTRACT

In external Compton scenario, we investigate the formation of the very hard electron spectrum in the fast-cooling regime, using a time-dependent emission model. It is shown that a very hard electron distribution  $N'_e(\gamma') \propto \gamma'^{-p}$  with the spectral index  $p \sim 1.3$  is formed below the minimum energy of injection electron when inverse Compton scattering takes place in the Klein-Nishina regime, i.e., inverse Compton scattering of relativistic electrons on broad-line region radiation in flat spectrum radio quasars. This produces a very hard gamma-ray spectrum, and can reasonably explain the very hard *Fermi*-LAT spectrum of the flat spectrum radio quasar 3C 279 during the extreme gamma-ray flare in 2013 December. We examine the impact of gamma-ray emission site on the evolution of electron distribution and their radiative output in detail. We find that such hard *Fermi*-LAT spectrum and simultaneous X-ray observations can put a stringent constraint on the gamma-ray emission site. Variability features in this scenario are simply discussed.

**Key words:** radiation mechanisms: non-thermal — galaxies: jets — gamma rays: galaxies

## 1 INTRODUCTION

Leptonic models have met with considerable successes in modelling the broadband (from radio to  $\gamma$ -ray frequencies) spectral energy distribution (SED) of all classes of blazars (e.g., Ghisellini et al. 2010; Zhang et al. 2012; Ghisellini et al. 2014). In leptonic models, non-thermal emission is produced by synchrotron emission of relativistic electrons in a comoving magnetic field and inverse Compton (IC) emission of relativistic electrons on low energy photons. For IC scattering, low-energy seed photons may be provided by synchrotron radiation (synchrotron-self Compton, SSC) and various external radiation fields (EC): (1) accretion disk radiation (EC-disk; Dermer & Schlickeiser 1993, 2002), (2) broad-line region (BLR) radiation (EC-BLR; Sikora et al. 1994), and (3) dust IR radiation (EC-dust; Błażejowski et al. 2000). Time-dependent leptonic models have been developed to study the observed variability features (e.g., Mastichiadis & Kirk. 1997; Li & Kusunose 2000; Kusunose et al. 2000; Böttcher & Chiang 2002; Böttcher & Dermer 2010; Chen et al. 2012; Saito et al. 2015).

Relativistic electron energy distribution (EED) is crucial for studying the non-thermal radiation from blazars. A static broken power-law EED (see Yan et al. 2013; Zhou et al. 2014, for constraining various EEDs with observations) is frequently used to model the SEDs of blazars (e.g., Tavecchio et al. 1998; Finke et al. 2008; Mankuzhiyil et al. 2011; Yan et al. 2012a, 2014; Zhang et al. 2014; Kang et al. 2014). An initial single power-law electron distribution can be deformed to become a broken power-law distribution due to radiative energy losses. In short, in the slow-cooling regime (i.e., the minimum energy of injected EED  $\gamma'_{\min}$  less than the broken energy  $\gamma'_b$  of cooled EED), the electron spectrum below  $\gamma'_b$  has a spectral index  $p = s$ , where  $s$  is the spectral index of the injected single power-law EED; above  $\gamma'_b$ , the spectrum is softened by cooling, and has an index  $s + 1$ . In the fast-cooling regime (i.e.,  $\gamma'_b = \gamma'_{\min}$ ),  $p \sim 2$ , independent of  $s$ ; above  $\gamma'_{\min}$ , the spectrum also has an index  $s + 1$  (e.g., Dermer & Menon 2009; Finke 2013). Note that standard shock acceleration theories predict  $s \sim 2$ . Modelling the SEDs of *Fermi*-LAT detected blazars (Abdo et al. 2010) returns a standard electron spectrum with  $p \sim 2$  below  $\gamma'_b$  (e.g., Yan et al. 2012a, 2014; Zhang et al. 2012; Kang et al. 2014).

However, the standard picture mentioned above faces challenges when trying to explain the very hard TeV emission detected for several high-synchrotron-peaked BL Lac

\* E-mail: yandahai@ihep.ac.cn

† E-mail: lizhang@ynu.edu.cn

‡ E-mail: zhangsn@ihep.ac.cn

objects (HSPs), e.g., 1ES 1101-232 and 1ES 0229+200. Various approaches have been proposed to explain the very hard TeV spectrum of HSPs: the leptonic models in extreme regime (e.g., Katarzyński et al. 2006; Tavecchio et al. 2009), the modified leptonic models in normal regime (e.g., Lefa et al. 2011; Böttcher et al. 2008; Yan et al. 2012b), and the Ultra-high energy cosmic rays propagation models (e.g., Essey et al. 2011; Murase et al. 2012; Yan et al. 2015).

The recently observed very hard GeV spectrum of the flat spectrum radio quasar (FSRQ) 3C 279 during an extreme  $\gamma$ -ray flare (Hayashida et al. 2015) also challenges the standard picture. Modeling by Hayashida et al. (2015) with a broken power-law EED showed that a very hard electron spectrum with  $p \sim 1$  below  $\gamma'_b \sim 3000$  is required to explain this very hard *Fermi*-LAT spectrum. In the slow-cooling regime, such a hard emitting electron spectrum requires special acceleration mechanisms to provide a very hard injection electron distribution, for example, magnetic reconnection (e.g., Zenitani & Hoshino 2001; Guo et al. 2014; Sironi & Spitkovsky 2014; Werner et al. 2014). Asano & Hayashida (2015) recently explained the very hard GeV spectrum in a stochastic acceleration model.

Here we study the formation of the very hard electron spectrum of FSRQs in the fast-cooling regime. We show that a very hard electron spectrum with  $p \sim 1.3$  below minimum injection energy is produced in the fast-cooling regime owing to IC scattering on BLR radiation in the Klein-Nishina (KN) regime. This produces very hard EC components, which can reasonably account for the very hard *Fermi*-LAT spectrum of 3C 279. In Section 2, we describe our model; numerical results are showed in Section 3. In Section 4, we apply our approach to the very *Fermi*-LAT spectrum of 3C 279. In Section 5, we give summary and discussion.

## 2 MODEL

### 2.1 Model Description

In a one-zone leptonic model, it is assumed that the emission is produced by relativistic electrons injected in a homogeneous blob of comoving radius  $R'$ . The emission blob moves with relativistic speed (corresponding to the bulk Lorentz factor  $\Gamma$ ) towards us. Due to the beaming effect, the observed emission is strongly boosted. For a blazar, we assume the Doppler factor  $\delta_D = \Gamma$ .

Relativistic electrons lose energy due to synchrotron and IC radiation. The kinetic equation governing the temporal evolution of the electrons distribution  $N'_e(\gamma', t')$  is

$$\frac{\partial N'_e(\gamma', t')}{\partial t'} = \frac{\partial}{\partial \gamma'} [\dot{\gamma}' N'_e(\gamma', t')] - \frac{N'_e(\gamma', t')}{t'_{\text{esc}}} + Q'(\gamma', t'), \quad (1)$$

where  $N'_e$  is the differential electron number and  $t'_{\text{esc}}$  the escape timescale.  $\dot{\gamma}'$  is the total cooling rate, and  $Q'(\gamma', t')$  is the electron injection rate.

We take into account two radiative cooling processes: synchrotron and EC. For FSRQs, the impact of SSC cooling on evolution of EED is negligible. The synchrotron cooling rate is given by

$$\dot{\gamma}'_{\text{syn}} = \frac{4c\sigma_T}{3m_e c^2} u_B \gamma'^2, \quad (2)$$

where

$$u_B = \frac{B'^2}{8\pi}$$

is the magnetic energy density and  $B'$  the comoving magnetic field,  $c$  is the speed of light,  $m_e$  is the electron mass, and  $\sigma_T$  is the Thomson cross section. A fairly accurate approximation for the EC cooling rate, valid in the Thomson through Klein-Nishina regimes, is given by Moderski et al. (2005), and it is

$$\dot{\gamma}'_{\text{EC}} = \frac{4c\sigma_T}{3m_e c^2} u'_0 \gamma'^2 f_{\text{KN}}(4\gamma'\epsilon'_0), \quad (3)$$

where  $u'_0$  and  $\epsilon'_0$  are the energy density and dimensionless photon energy, respectively, of the external radiation field in the comoving frame of blob. The correction function for KN effect is given by

$$f_{\text{KN}}(x) = \frac{1}{(1+x)^{1.5}}. \quad (4)$$

The external radiation includes emissions from broad-line region (BLR) and infrared dust torus. Their energy densities in the comoving frame as the functions of the distance  $r$  from the black hole are given by (Sikora et al. 2009; Hayashida et al. 2012)

$$u'_{\text{BLR}}(r) = \frac{\Gamma^2 \tau_{\text{BLR}} L_{\text{disk}}}{3\pi r_{\text{BLR}}^2 c [1 + (r/r_{\text{BLR}})^3]}, \quad (5)$$

$$u'_{\text{dust}}(r) = \frac{\Gamma^2 \tau_{\text{dust}} L_{\text{disk}}}{3\pi r_{\text{dust}}^2 c [1 + (r/r_{\text{dust}})^4]}, \quad (6)$$

where  $\tau_{\text{BLR}}$  and  $\tau_{\text{dust}}$  are the fractions of the disk luminosity reprocessed into BLR radiation and into dust radiation, respectively. The typical values of  $\tau_{\text{BLR}} = 0.1$  (e.g., Ghisellini et al. 2014) and  $\tau_{\text{dust}} = 0.3$  (e.g., Hao et al. 2005; Malmrose et al. 2011) are adopted in the following calculations. The sizes of BLR and dust torus are related to the disk luminosity  $L_{\text{disk}}$  (Ghisellini & Tavecchio 2009; Ghisellini et al. 2014), i.e.,

$$r_{\text{BLR}} = 10^{17} (L_{\text{disk}}/10^{45} \text{ erg s}^{-1})^{1/2} \text{ cm}, \quad (7)$$

$$r_{\text{dust}} = 10^{18} (L_{\text{disk}}/10^{45} \text{ erg s}^{-1})^{1/2} \text{ cm}. \quad (8)$$

Then, we have

$$u'_{\text{BLR}}(r) \simeq \frac{0.3\Gamma^2 \tau_{\text{BLR}}}{1 + (r/r_{\text{BLR}})^3} \text{ erg cm}^{-3}, \quad (9)$$

$$u'_{\text{dust}}(r) \simeq \frac{0.003\Gamma^2 \tau_{\text{dust}}}{1 + (r/r_{\text{dust}})^4} \text{ erg cm}^{-3}. \quad (10)$$

Therefore,  $u'_0$  is also a function of  $r$ , i.e.,

$$u'_0(r) = u'_{\text{dust}}(r) + u'_{\text{BLR}}(r). \quad (11)$$

BLR (IR dust) radiation is assumed to be a diluted blackbody radiation. Given that BLR radiation is dominated by Ly $\alpha$  line photons, we adopt an effective temperature for the BLR radiation of  $T_{\text{BLR}} = 4.2 \times 10^4$  K, so that the energy density of BLR radiation peaks at  $\approx 2.82 k_B T_{\text{BLR}}/h \cong 2.5 \times 10^{15}$  Hz (corresponding to the mean dimensionless energy  $\epsilon_{\text{BLR}} = 2 \times 10^{-5}$ ). We assume an effective temperature for

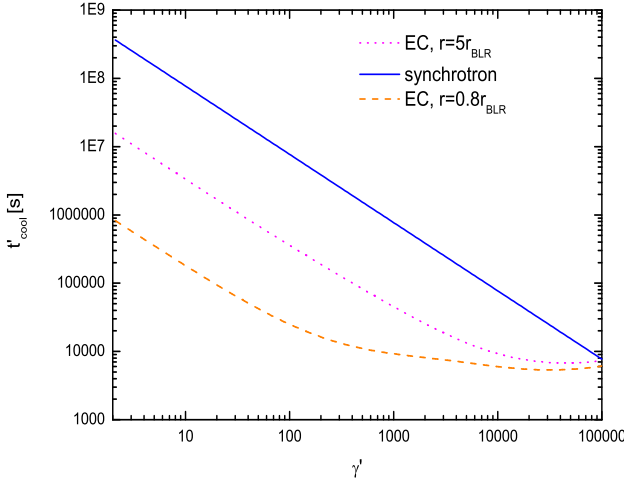


**Figure 1.** Cooling time for synchrotron radiation and EC processes.  $B' = 1$  G and  $\Gamma = 30$  are used.

the IR dust radiation of  $T_{\text{dust}} = 1000$  K (Malmrose et al. 2011), i.e., the mean dimensionless energy  $\epsilon_{\text{dust}} = 5 \times 10^{-7}$ . Then we have  $\epsilon'_0 = \Gamma \epsilon_{\text{BLR}}$  for  $r \leq 2r_{\text{BLR}}$ , and  $\epsilon'_0 = \Gamma \epsilon_{\text{dust}}$  for  $r > 2r_{\text{BLR}}$ .

The total cooling rate from synchrotron and EC losses is

$$\dot{\gamma}'(r) = \dot{\gamma}'_{\text{syn}} + \dot{\gamma}'_{\text{EC}}(r). \quad (12)$$

We neglect the electron energy loss due to adiabatic expansion, because in FSRQs the adiabatic cooling with an expanding velocity  $\sim 0.1c$  is relevant only for very low energy electrons, which do not contribute to the radiative output.

In Fig. 1, we show the cooling time ( $\gamma'/\dot{\gamma}'$ ) for synchrotron radiation and EC processes. We use  $B' = 1$  G,  $\Gamma = 30$  and  $L_{\text{disk}} = 1.5 \times 10^{45}$  erg s $^{-1}$ . One can find that taking  $r = 0.8 r_{\text{BLR}}$ , significant KN correction takes place at  $\gamma' \gtrsim 1/4\Gamma\epsilon_{\text{BLR}} \sim 400$ ; taking  $r = 5 r_{\text{BLR}}$ , the KN correction takes place at  $\gamma' > 10^4$ .

We consider a constant injection during the injection time  $t'_{\text{inj}}$ . The injection electron distribution is

$$Q'(\gamma') = Q'_0 \gamma'^{-s} \exp(-\gamma'/\gamma'_{\text{cut}}) H(\gamma'; \gamma'_{\text{min}}), \quad (13)$$

where  $s$  is the spectral index,  $\gamma'_{\text{min}}$  is the minimum injection energy,  $\gamma'_{\text{cut}}$  is the cut-off energy, and  $Q'_0$  [s $^{-1}$ ] is the normalization constant;  $H(\gamma'; \gamma'_{\text{min}}) = 1$  for  $\gamma' > \gamma'_{\text{min}}$ , otherwise  $H(\gamma'; \gamma'_{\text{min}}) = 0$ .

We naturally relate  $r$  to time by:

$$r = r_0 + ct'\Gamma, \quad (14)$$

where  $r_0$  is the distance where the injection starts.

### 3 NUMERICAL RESULTS

We numerically solve equation (1), adopting the numerical method given by Chiaberge & Ghisellini (1999). In

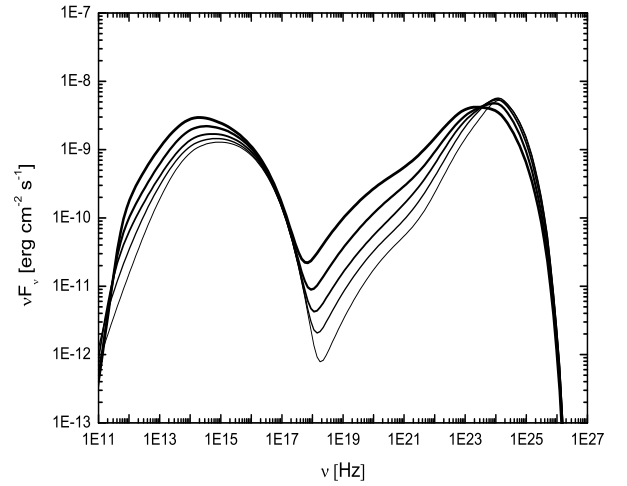
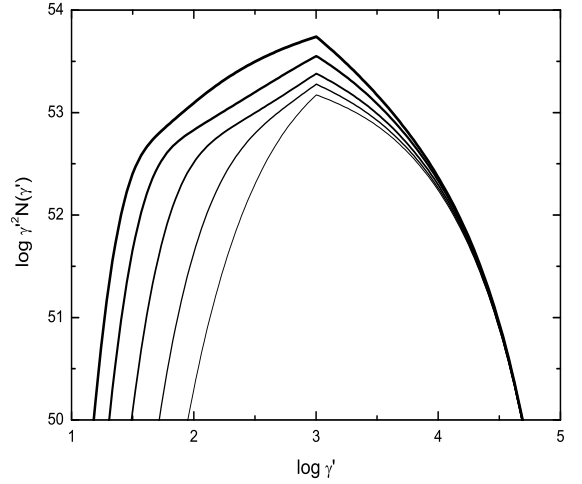


**Figure 2.** Temporal evolution of EED (top panel) and SED (bottom panel) with  $r_0 = 0.8r_{\text{BLR}}$ . The lines from thin to heavy correspond to  $t' = [1.5, 3, 6, 12, 24] \times 10^4$  s, respectively. We use  $\gamma'_{\text{min}} = 10^3$ ,  $\gamma'_{\text{cut}} = 10^4$ ,  $Q_0 = 4.8 \times 10^{49}$  s $^{-1}$ ,  $s = 2.1$ ,  $B' = 1$  G,  $\delta_D = 30$ ,  $R' = 10^{16}$  cm, and  $L_{\text{disk}} = 1.5 \times 10^{45}$  erg s $^{-1}$ .

the calculations, we use  $t'_{\text{esc}} = t'_{\text{inj}} = 10^8$  s. We calculate the synchrotron and IC spectra using the methods given by Dermer & Menon (2009). Synchrotron-self absorption is taken into account. We use parameters  $H_0 = 71$  km s $^{-1}$  Mpc $^{-3}$ ,  $\Omega_m = 0.27$ ,  $\Omega_\Lambda = 0.73$ , and the redshift  $z = 0.536$  for 3C 279.

#### 3.1 Results in fast-cooling regime

In Fig. 2, we show the temporal evolution of EED and SED in the case of the emission region initially located inside BLR. One can see that EED develops a very hard  $N'_e(\gamma') \propto \gamma'^{-1.3}$  form below the minimum injection energy. This very hard spectrum is different from the standard shape

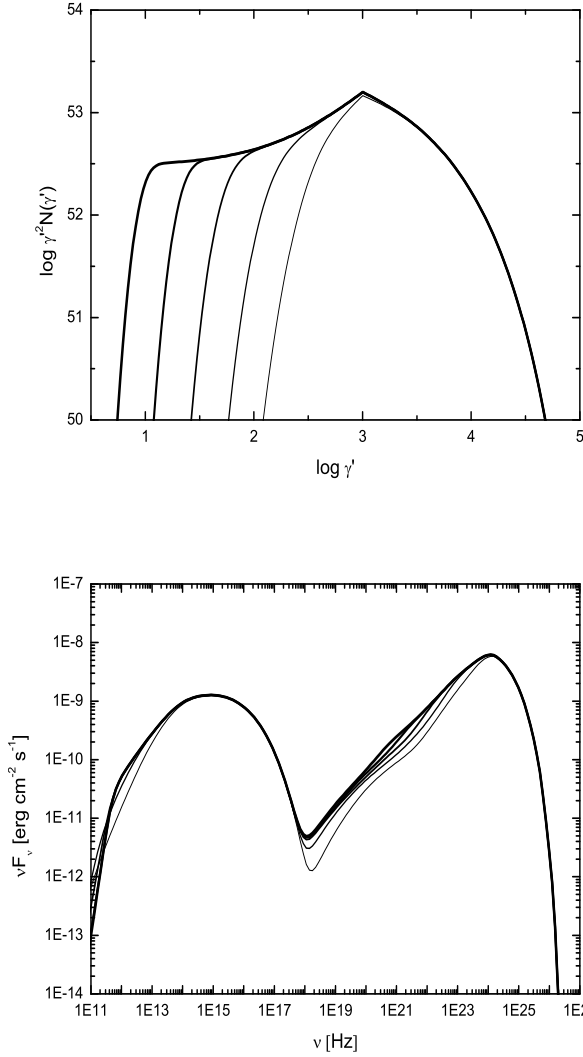


**Figure 3.** Same as Fig. 2, but with  $r = 0.8r_{\text{BLR}}$ .

of  $N'(\gamma') \propto \gamma'^{-2}$  expected in the case of Thomson or synchrotron cooling processes of the form  $\dot{\gamma}' \propto \gamma'^2$ . The hardening in the electron spectrum is mainly owing to KN energy losses on the BLR radiation. The minimum energy  $\gamma'_1$  of the emitting electron distribution is affected by the evolution time  $t'$  when  $t' < t'_{\text{esc}}$ , which can be evaluated by the relation  $t'_{\text{cool}} = t'$ . In the fast-cooling regime, we have  $\gamma'_1 < \gamma'_{\text{min}}$ . The  $\gamma$ -ray spectrum in Fig. 2 is the sum of EC-BLR and EC-dust components. Below  $\sim 10^{24}$  Hz, we have a very hard  $\gamma$ -ray spectrum. When the emission region moves outside BLR, i.e.,  $t' > 1.2 \times 10^5$  s, a softening in EED and SED occurs. Actually, the shape of EED below  $\gamma'_{\text{min}}$  determines the shape of EC spectrum between  $2\epsilon'_0\delta_D\gamma_1^2$  to  $2\epsilon'_0\delta_D\gamma_{\text{min}}^2$  in the Thomson regime, i.e.,  $\nu F_\nu \propto \nu^{(3-p)/2}$  (Dermer & Menon 2009), where  $p$  is the spectral index of the electron spectrum below  $\gamma'_{\text{min}}$ .

One can see that the variation in EED with time is significant below  $\gamma'_{\text{cut}}$  (see top panels in Figs. 2). The change

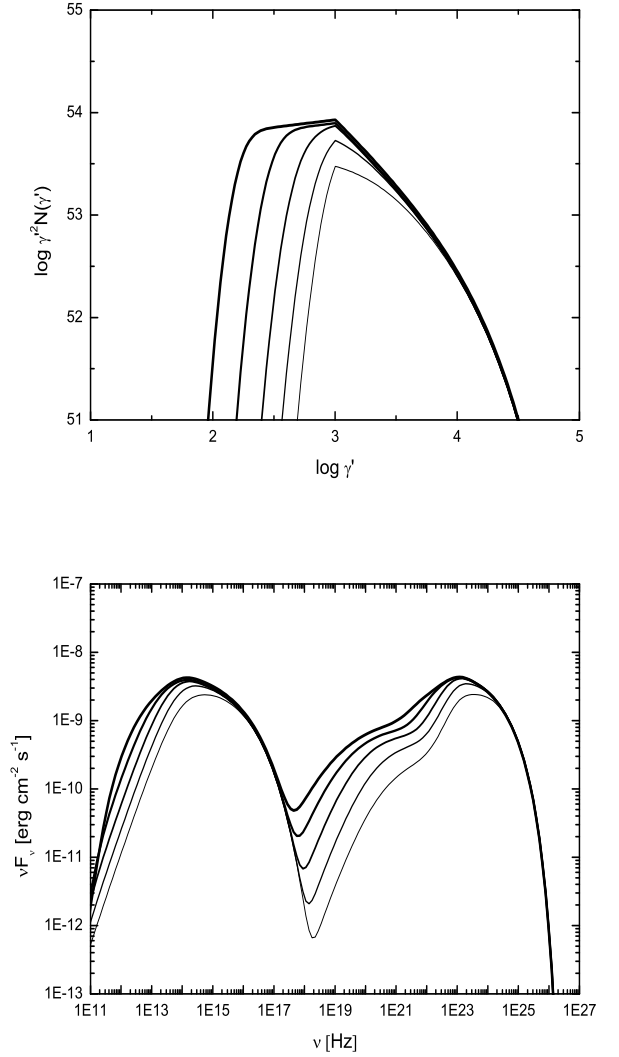


**Figure 4.** Temporal evolution of EED (top panel) and SED (bottom panel) with  $r_0 = 5r_{\text{BLR}}$ . The lines from thin to heavy correspond to  $t' = [1.5, 3, 6, 12, 24] \times 10^4$  s, respectively. The other parameters are same as those in Fig. 2.

in EED leads to the change in synchrotron spectrum below  $\sim 4 \times 10^6 B' \gamma_{\text{cut}}'^2 \delta_D$  Hz, and the change in EC spectrum below  $\sim 10^{20} \epsilon'_0 \delta_D \gamma_{\text{cut}}'^2$  Hz. Note that the change in EC spectrum between  $\sim 10^{20} \epsilon'_0 \delta_D \gamma_{\text{KN}}'^2$  Hz and  $\sim 10^{20} \epsilon'_0 \delta_D \gamma_{\text{cut}}'^2$  Hz will be suppressed by the KN effect, where  $\gamma'_{\text{KN}} \sim 1/4\epsilon'_0$ . The variation of the X-ray spectrum is due to the change of  $\gamma'_1$ .

In above calculations, the energy density of BLR varies with time because  $r \sim r_{\text{BLR}}$ . In Fig. 3, we show the results for a constant energy density of BLR (corresponding to  $r < r_{\text{BLR}}$ ) by fixing  $r = r_0$ . In this case the electron distribution above  $\gamma'_{\text{min}}$  does not vary with time (see top panel in Fig. 3). Below  $\gamma'_{\text{min}}$ , the distribution obviously hardens at  $\sim 1/4\Gamma\epsilon_{\text{BLR}}$ . When  $\gamma'_1 \ll 1/4\Gamma\epsilon_{\text{BLR}}$ , there is a clear shape  $N'_e(\gamma') \propto \gamma'^{-2}$  between  $\gamma'_1$  and  $\gamma' \sim 100$ . Looking at the

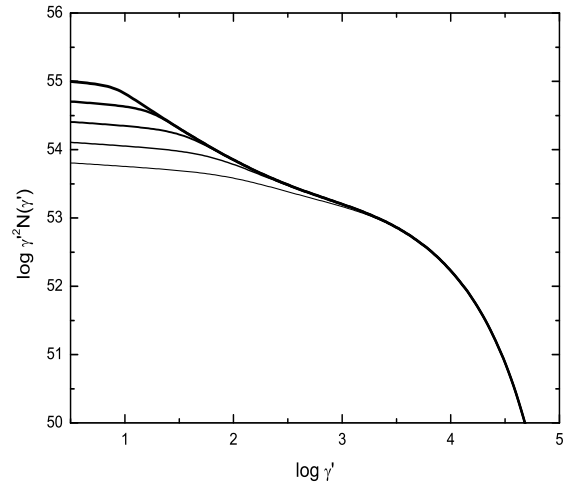
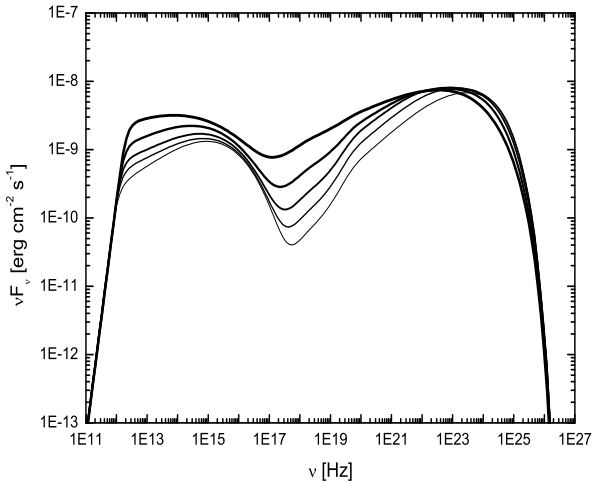
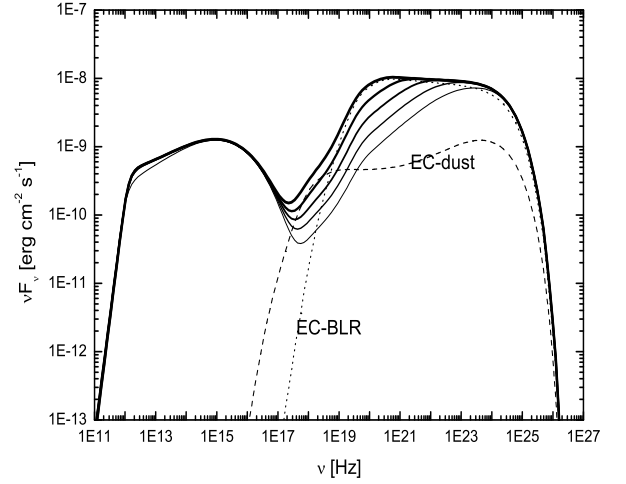
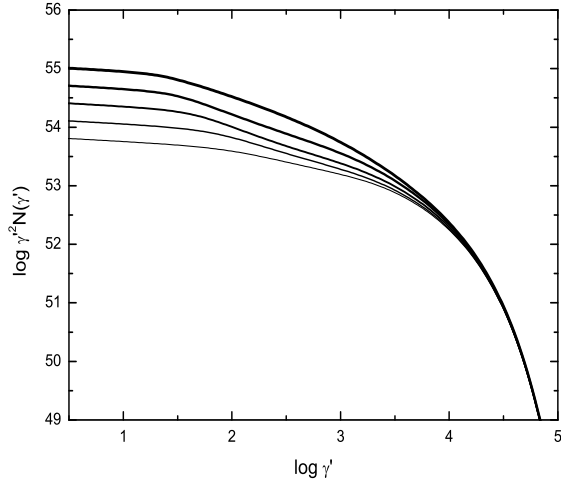


**Figure 5.** Same as Fig. 2, but with  $\gamma'_{\min} = 3$ , corresponding to the slow-cooling scenario.

evolution of SED, the multifrequency emissions are weakly variable.

From Fig. 2 and Fig. 3, one can see that optical and X-ray observations can distinguish the above two scenarios. Namely, a very hard *Fermi*-LAT spectrum and simultaneous X-ray/optical observations can put a very strong constraint on the  $\gamma$ -ray emission site.

In Fig. 4, we show the temporal evolution of EED and SED in the case of the emission region located far beyond the BLR. As expected, a standard shape  $N'_e(\gamma') \propto \gamma'^{-2}$  is formed below  $\gamma'_{\min}$ . The  $\gamma$ -ray spectrum is also softer than that in Fig. 2.

### 3.2 Results in slow-cooling regime

For comparison, we revisit the KN effect in the slow-cooling region (e.g., Dermer & Atoyan 2002; Kusunose & Takahara

**Figure 6.** Same as Fig. 5, but with  $r = 0.8r_{\text{BLR}}$ .

2005; Georganopoulos et al. 2006). In Figs. 5 and 6, we show the results in the slow-cooling regime; no very hard electron spectrum with  $p < 2$  is seen. In a constant BLR radiation case (Fig. 6), it is clear that the EED hardens from  $N'_e(\gamma') \propto \gamma'^{-(s+1)}$  ( $s = 2.1$ ) in the Thomson regime to  $N'_e(\gamma') \propto \gamma'^{-2.5}$  in the KN regime. This produces a flattening in the EC spectrum (see bottom panel in Fig. 6). This situation is very similar to the flattening in EC spectrum in FSRQs shown by Georganopoulos et al. (2006) and the flattening in synchrotron X-ray spectrum in extended *Chandra* jet presented by Dermer & Atoyan (2002).

## 4 APPLICATION TO THE VERY HARD $\gamma$ -RAY SPECTRUM OF 3C 279

We apply our approach to the very hard spectrum with photon spectral index  $\Gamma_\gamma \simeq 1.7$  of 3C 279 during an extreme

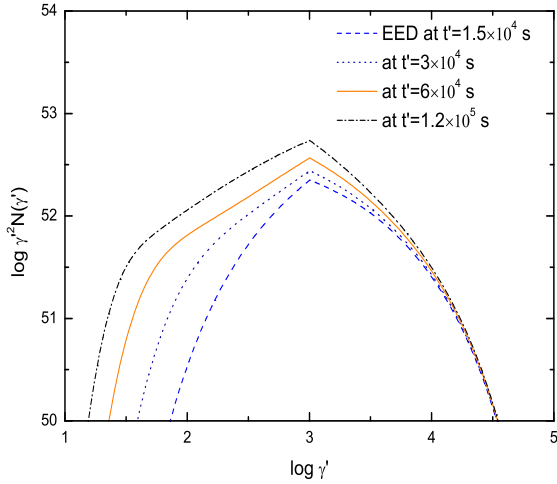
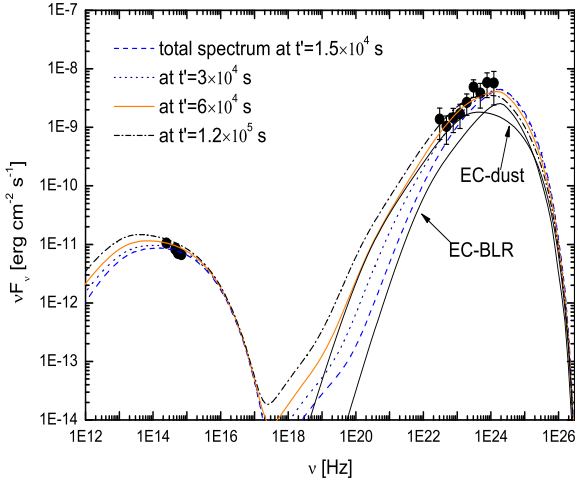


**Figure 7.** Modeling the very hard  $\gamma$ -ray spectrum of 3C 279 during 2013 December. Top: SEDs; bottom: corresponding EEDs. The parameters are  $t'_{\text{inj}} = 10^8$  s,  $\gamma'_{\text{min}} = 10^3$ ,  $\gamma'_{\text{cut}} = 10^4$ ,  $B' = 0.11$  G,  $\delta_D = 42$ ,  $R' = 7.5 \times 10^{15}$  cm,  $Q_0 = 9.5 \times 10^{48}$  s $^{-1}$ ,  $s = 2.1$ , and  $r_0 = 0.8 r_{\text{BLR}}$ .

flare (Hayashida et al. 2015). The variability timescale of the  $\gamma$ -ray flare is estimated to be  $t_{\text{var}} \simeq 2$  hr (Hayashida et al. 2015). This timescale is used to constrain the radius of the emission blob,  $R' \lesssim ct_{\text{var}}\delta_D/(1+z)$ . We use  $L_{\text{disk}} = 1.5 \times 10^{45}$  erg s $^{-1}$  (Yan, Zhang & Zhang 2015), then we have  $r_{\text{BLR}} = 1.2 \times 10^{17}$  cm. We assume  $t'_{\text{esc}} = 10^8$  s.

A satisfactory fit to the very hard  $\gamma$ -ray spectrum as well as the optical data is seen in Fig. 7; model parameters can be found in the caption of Fig. 7. No extreme parameter is required. The distance where the injection starts is comparable to the size of the BLR,  $r_0 = 0.8 r_{\text{BLR}}$ . The magnetic field is well below that in other activities derived by Dermer et al. (2014) and Yan, Zhang & Zhang (2015); Yan et al. (2015) who used a static log-parabola EED to model the SEDs

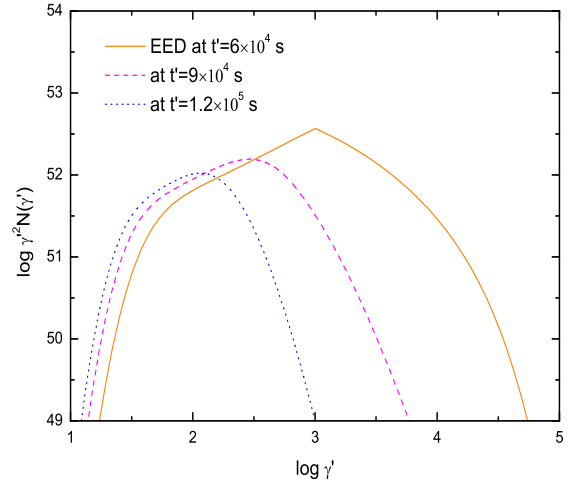
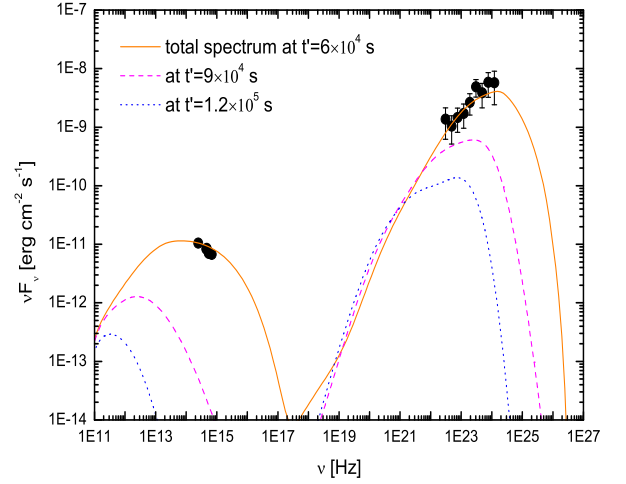


**Figure 8.** Same as Fig. 7, but using  $t'_{\text{inj}} = 7 \times 10^4$  s.

of 3C 279. The comoving frame electron injection power is  $L'_{\text{inj}} = 6.2 \times 10^{42}$  erg s $^{-1}$ . The EED develops a clear form of  $N'_e(\gamma') \propto \gamma'^{-1.3}$  below  $\gamma'_{\text{min}}$  when  $t' > 1.5 \times 10^4$  s; above  $\gamma'_{\text{min}}$ , the spectral index increases from  $\sim 2.6$  to  $3.0$  from  $t' = 1.5 \times 10^4$  s to  $1.2 \times 10^5$  s, which is caused by the varying  $u_{\text{BLR}}$  when  $r \sim r_{\text{BLR}}$  (see the examinations in Section 3.1).

In this model, the portion of the  $\gamma$ -ray spectrum below  $\sim 1$  GeV is almost entirely from Compton scattering of dust IR photons, while above  $\sim 1$  GeV it is from Compton scattering of a combination of BLR and dust radiation.

From the temporal evolution of the SED in Fig. 7, we can see that optical and  $\gamma$ -ray emissions are weakly variable when  $t' < t'_{\text{inj}}$ , while X-rays are strongly variable. X-rays lag  $\gamma$  rays and optical emission.

In Fig. 8, one can see the temporal evolutions of the SED and EED when  $t' > t'_{\text{inj}}$ . Both optical and  $\gamma$ -ray emissions dramatically decrease when  $t' > t'_{\text{inj}}$ . It is noted that



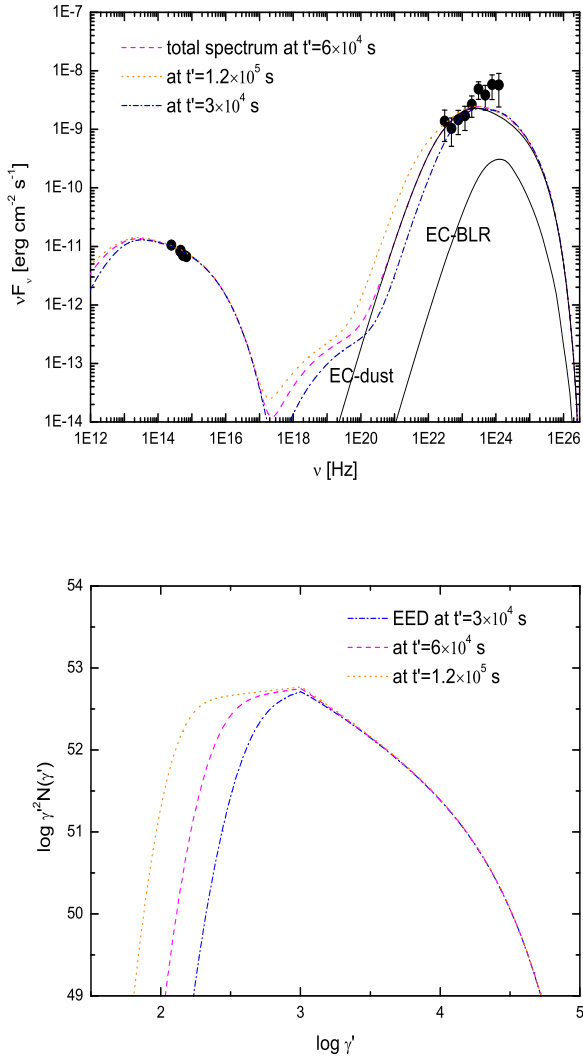


**Figure 9.** Same as Fig. 7, but with  $Q_0 = 7.0 \times 10^{48} \text{ s}^{-1}$  and  $r_0 = 3 r_{\text{BLR}}$ .

the optical emission soon becomes undetectable after stopping the injection (see top panel in Fig. 8), while the  $\gamma$ -ray emission keeps detectable for some time after stopping the injection. We note that the EED is quickly narrowed after stopping the injection.

In Fig. 9, we show the modeling results with  $r_0 = 3r_{\text{BLR}}$ . In this case, the model cannot account for the  $\gamma$ -ray data above 1 GeV. The spectral index of electron spectrum above  $\gamma' > \gamma'_{\text{min}}$  is  $\approx 3.2$ , resulting in a  $\gamma$ -ray spectrum of  $\nu F_\nu \propto \nu^{-0.1}$  above 0.5 GeV which is softer than the observed spectrum.

Comparing the results in Figs. 7 and Fig. 9, we notice that the more intense energy density of BLR radiation results in a smaller  $\gamma'_1$ , which causes a more substantial contribution of EC to X-ray emission.

## 5 SUMMARY AND DISCUSSION

We have fully investigated the evolution of the EED in the jet of FSRQs using a time-dependent model. We found that a very hard electron spectrum with  $p \sim 1.3$  below minimum injection energy is formed in the fast-cooling scenario owing to Compton scattering BLR radiation in the KN regime. This produces a very hard spectrum up to  $\sim 5$  GeV via inverse Compton scattering BLR and dust radiations.

We also examined the impact of the  $\gamma$ -ray emission site on the formation of EED in detail. We relate the  $\gamma$ -ray emission site  $r$  to time in a natural way (see equation 14). If  $r \sim r_{\text{BLR}}$ , the energy density of BLR is also time-dependent (see equation 9); whereas if  $r \ll r_{\text{BLR}}$ , the energy density of BLR is constant. We showed that the EEDs formed in the two cases are different (see Fig. 2 and Fig. 3), and the differences between EEDs result in clear differences between the X-ray emissions. In particular, the X-rays in the former case are strongly variable (see Fig. 2), while in the latter case both X-rays and  $\gamma$  rays are weakly variable (see Fig. 3). Hence we suggest that such very hard  $\gamma$ -ray spectrum and simultaneous X-ray data can put a very strong constraint on the  $\gamma$ -ray emission site.

The impacts of IC scattering in the KN regime on EED have been investigated by previous studies in the slow-cooling scenario (e.g., Dermer & Atoyan 2002; Kusunose & Takahara 2005; Georganopoulos et al. 2006; Sikora et al. 2009). For comparison, we also revisited this scenario. We showed that, in the slow-cooling scenario, the electron distribution becomes harder at  $\sim \gamma'_{\text{KN}}$  with the spectral index from  $\sim s + 1$  ( $s = 2.1$  is the index of injection spectrum) to  $\sim 2.5$ . This moderate hardening in EED results in a flat EC-BLR/dust component, which is similar to the finding in Georganopoulos et al. (2006), also see the results in Dermer & Atoyan (2002). We do not see a dip in  $\gamma'^2 N_e(\gamma')$  distribution presented by Kusunose & Takahara (2005). We note that Kusunose & Takahara (2005) also obtained a similar flat EC component. However, the formation mechanisms for such flat spectrum in the *Fermi*-LAT energy range are not unique.

As we showed, our model can reasonably explain the very hard  $\gamma$ -ray spectrum of 3C 279 observed in the extreme flare during 2013 December. The satisfactory modelling is sensitive to the  $\gamma$ -ray emission site, and requires the  $\gamma$ -ray emission taking place inside the BLR or at the edge of BLR. Our model expects that X-rays lag optical and  $\gamma$ -ray emission, which can be tested by future observations. A more complicated injection rate might be needed to reproduce the  $\gamma$ -ray light-curve profile. During the extreme  $\gamma$ -ray flare, the optical emission showed weak variability (Hayashida et al. 2015). The problem of lack of simultaneous optical variability might be resolved in the fast-cooling regime where the electrons making optical emission by synchrotron radiation do not make a substantial contribution to the LAT spectrum.

Hayashida et al. (2015) showed that a very hard electron spectrum with  $p \simeq 1$  below  $\gamma' \lesssim 3000$  is required for explaining the LAT spectrum of 3C 279 during the extreme  $\gamma$ -ray flare. In the slow-cooling regime, a special acceleration mechanism should be taken into account to explain such hard EED. Recent studies demonstrated that particles can be efficiently accelerated to develop non-thermal distribu-

tions with a spectral index  $\sim 1$  in the magnetic reconnection scenario (Sironi & Spitkovsky 2014; Guo et al. 2014, 2015). In the fast-cooling regime, we can avoid the requirement of a special acceleration mechanism.

The difference between the cooling behaviours in the Thomson and KN regimes not only affects the EED/ $\gamma$ -ray spectrum, but also affects the decay of  $\gamma$ -ray light curve. In the KN regime, cooling time is energy-independent, while in the Thomson regime cooling time is energy-dependent. This difference has been proposed to constrain the  $\gamma$ -ray emission site in FSRQs (Dotson et al. 2012, 2015).

It is interesting to note that the mean  $\Gamma_\gamma$  for the *Fermi*-LAT detected FSRQs is  $2.44 \pm 0.20$  (Ackermann et al. 2015). Analyses of the  $\gamma$ -ray spectra with  $\Gamma_\gamma > 2$  and the simultaneous optical and X-ray data indicated that  $\gamma$ -ray emissions of 3C 279 take place outside the BLR (Dermer et al. 2014; Paliya 2015; Yan, Zhang & Zhang 2015; Yan et al. 2015). Pacciani et al. (2014) also found the evidence of gamma-ray flares occurring outside the BLR in ten FSRQs.

As a last remark, we note that very recently Uhm & Zhang (2014) and Zhao et al. (2014) showed that a very hard electron spectrum with  $p \sim 1$  can be produced in the fast-cooling regime due to synchrotron radiation in a strongly decaying magnetic field. This can explain the  $\gamma$ -ray burst (GRB) prompt emission spectra whose low-energy photon spectral index has a value  $\sim 1$ .

## ACKNOWLEDGMENTS

We are grateful to Krzysztof Nalewajko for providing us the data of 3C 279. We thank Xiang-Yu Wang and Zhuo Li for bringing this KN effect in GRB study (e.g., Wang et al. 2009) to our attention when this work is presented at the 8th black hole conference, held in Kunming 14 - 16th October 2015. This work is partially supported by the National Natural Science Foundation of China (NSFC 11433004) and Top Talents Program of Yunnan Province, China. DHY acknowledges funding support by China Postdoctoral Science Foundation under grant No. 2015M570152, and by the National Natural Science Foundation of China (NSFC) under grant No. 11573026. SNZ acknowledges partial funding support by 973 Program of China under grant 2014CB845802, by the National Natural Science Foundation of China (NSFC) under grant Nos. 11133002 and 11373036, by the Qianren start-up grant 292012312D1117210, and by the Strategic Priority Research Program “The Emergence of Cosmological Structures” of the Chinese Academy of Sciences (CAS) under grant No. XDB09000000.

## REFERENCES

Abdo A. A., Ackermann M., Ajello M., et al., 2010, *ApJ*, 716, 30  
 Ackermann M., Ajello M., Atwood W., et al., 2015, *ApJ*, 810, 14  
 Asano K., Hayashida M., 2015, *ApJL*, 808, 18  
 Błażejowski M., Sikora M., Moderski R., Madejski G. M., 2000, *ApJ*, 545, 107  
 Böttcher M., Chiang J., 2002, *ApJ*, 581, 127  
 Böttcher M., Dermer C. D., Finke J. D. 2008, *ApJ*, 679, L9  
 Böttcher M., Dermer C. D., 2010, *ApJ*, 711, 445  
 Chen X. H., Fossati G., Böttcher M., Liang E., *MNRAS*, 424, 789  
 Chiaberge M., Ghisellini G., 1999, *MNRAS*, 306, 551

Dermer C. D., Schlickeiser R., 1993, *ApJ*, 416, 458  
 Dermer C. D., Schlickeiser R., 2002, *ApJ*, 575, 667  
 Dermer C. D., Atoyan, A. M., 2002, *ApJ*, 568, L81  
 Dermer C. D., Menon, G. 2009, *High Energy Radiation from Black Holes* (Princeton University Press)  
 Dermer C. D., Cerruti M., Lott B., Boisson C., Zech A., 2014, *ApJ*, 782, 82  
 Dotson A., Georganopoulos M., Kazanas D., Perlman E. S., 2012, *ApJ*, 758, L15  
 Dotson A., Georganopoulos M., Meyer E. T., McCann K., 2015, *ApJ*, 809, 164  
 Essey W., Kalashev O. E., Kusenko A., Beacom J. F., 2011, *ApJ*, 731, 51  
 Finke J. D., Dermer C. D., Böttcher M., 2008, *ApJ*, 686, 181  
 Finke J. D., *ApJ*, 763, 134  
 Georganopoulos M., Perlman E. S., Kazanas D., & Wingert B., 2006, in *ASP Conf. Ser. 350, Blazar Variability Workshop II: Entering the GLAST Era*, ed. H. R. Miller, K. Marshall, J. R. Webb, & M. F. Aller (San Francisco, CA: ASP), 178  
 Ghisellini G., Tavecchio F., 2009, *MNRAS*, 397, 958  
 Ghisellini G., Tavecchio F., Foschini L., et al., 2010, *MNRAS*, 402, 497  
 Ghisellini G., Tavecchio F., Maraschi L., Celotti A., Sbarbato T., 2014, *Nature*, 515, 376  
 Guo F., Li H., Daughton W., Liu Y.-H., 2014, *Physical Review Letters*, 113, 155005  
 Guo F., Liu Y.-H., Daughton W., Li H., 2015, *ApJ*, 806, 167  
 Hao L., et al., 2005, *AJ*, 129, 1795  
 Hayashida M., Madejski G. M., Nalewajko K., et al., 2012, *ApJ*, 754, 114  
 Hayashida M., Nalewajko K., Madejski G. M., et al. 2015, *ApJ*, 807, 79  
 Kang S. J., Chen L., Wu Q. W., 2014, *ApJS*, 215, 5  
 Katarzyński K., Ghisellini G., Tavecchio F., Gracia J., & Maraschi L. 2006, *MNRAS*, 368, L52  
 Kusunose M., Takahara F., & Li H., 2000, *ApJ*, 536, 299  
 Kusunose M., & Takahara F., 2005, *ApJ*, 621, 285  
 Li H., & Kusunose M., 2000, *ApJ*, 536, 729  
 Lefa E., Rieger F. M., & Aharonian F., 2011, *ApJ*, 740, 64  
 Malmrose M. P., Marscher A. P., Jorstad S. G., Nikutta R., Elitzur M., 2011, *ApJ*, 732, 116  
 Mankuzhiyil N., Ansoldi S., Persic M., Tavecchio F., 2011, *ApJ*, 733, 14  
 Mastichiadis A., & Kirk J. G. 1997, *A&A*, 320, 19  
 Moderski R., Sikora M., Coppi P. S., & Aharonian, F., 2005, *MNRAS*, 363, 954  
 Murase K., Dermer C. D., Takami H., Migliori G., 2012, *ApJ*, 749, 63  
 Pacciani L., Tavecchio F., Donnarumma I., et al., 2014, *ApJ*, 790, 45  
 Paliya V. S., 2015, *ApJL*, 808, 48  
 Sikora M., Begelman M. C., Rees M. J., 1994, *ApJ*, 421, 153  
 Sikora M., Stawarz L., Moderski R., Nalewajko K., Madejski G. M., 2009, *ApJ*, 704, 38  
 Saito S., Stawarz L., Tanaka Y. T., Takahashi T., Sikora M., Moderski R., 2015, *ApJ*, 809, 171  
 Sironi, L., Spitkovsky, A. 2014, *ApJL*, 783, L21  
 Tavecchio F., Maraschi L., Ghisellini G., 1998, *ApJ*, 509, 608  
 Tavecchio F., Ghisellini G., Ghirlanda G., Costamante L., Franceschini A., 2009, *MNRAS*, 399, L59  
 Uhm Z. L., Zhang B., 2014, *NatPh*, 10, 351  
 Wang X. Y., Li Z., Dai, Z. G., Mészáros P., 2009, *ApJ*, 698, L98  
 Werner, G. R., Uzdensky, D. A., Cerutti, B., Nalewajko, K., & Begelman, M. C. 2014, *arXiv:1409.8262*  
 Yan D. H., Zeng H. D., Zhang L., 2012a, *PASJ*, 64, 80  
 Yan D. H., Zeng H. D., Zhang L., 2012b, *MNRAS*, 424, 2173  
 Yan D. H., Zhang L., Yuan Q., Fan Z. H., Zeng H. D., 2013, *ApJ*, 765, 122



- Yan D. H., Zeng H. D., Zhang L., 2014, MNRAS, 439, 2933  
Yan D. H., Kalashev O., Zhang L., Zhang S. N., 2015, MNRAS, 449, 1018  
Yan D. H., Zhang L., Zhang S. N., 2015, MNRAS, 454, 1310  
Yan D. H., He, J. J., Liao, J. Y., Zhang L., Zhang S. N., 2015, arxiv: 1510.03118  
Zenitani S., Hoshino M., 2001, ApJ, 562, L63  
Zhao X. H., Li Z., Liu X. W., Zhang B. B, Bai J. M., Mészáros P. , 2014, ApJ, 780, 12  
Zhang J., Liang E. W., Zhang S. N., Bai, J. M., 2012, ApJ, 752, 157  
Zhang J., Sun X. N., Liang E. W., Lu R., J., Lu Y., Zhang S. N., 2014, ApJ, 788, 104  
Zhou Y., Yan D. H., Dai B. Z., Zhang L., 2014, PASJ, 66, 12

This paper has been typeset from a  $\text{\TeX}/\text{\LaTeX}$  file prepared by the author.

